

# Nanoscale

Accepted Manuscript



This is an *Accepted Manuscript*, which has been through the Royal Society of Chemistry peer review process and has been accepted for publication.

*Accepted Manuscripts* are published online shortly after acceptance, before technical editing, formatting and proof reading. Using this free service, authors can make their results available to the community, in citable form, before we publish the edited article. We will replace this *Accepted Manuscript* with the edited and formatted *Advance Article* as soon as it is available.

You can find more information about *Accepted Manuscripts* in the [Information for Authors](#).

Please note that technical editing may introduce minor changes to the text and/or graphics, which may alter content. The journal's standard [Terms & Conditions](#) and the [Ethical guidelines](#) still apply. In no event shall the Royal Society of Chemistry be held responsible for any errors or omissions in this *Accepted Manuscript* or any consequences arising from the use of any information it contains.

# Transparent Conductors Composed of Nanomaterials

Michael Layani, Alexander Kamyshny and Shlomo Magdassi

Received (in XXX, XXX) Xth XXXXXXXXXX 20XX, Accepted Xth XXXXXXXXXX 20XX

DOI: 10.1039/b000000x

This is a review on recent developments in the field of transparent conductive coatings (TCCs) for ITO replacement. The review describes the basic properties of conductive nanomaterials suitable for fabrication of such TCCs (metallic nanoparticles and nanowires, carbon nanotubes and graphene sheets), various methods of patterning the metal nanoparticles with formation of conductive transparent metallic grids, honeycomb structures and 2D arrays of interconnected rings as well as fabrication of TCCs based on graphene and carbon nanotubes. Applications of TCCs for electronic and optoelectronic devices, such as solar cells, electroluminescent and electrochromic devices, touch screens and displays, and transparent EMI shielders are presented.

## 1. Introduction

Nowadays, most people encounter optoelectronic devices, such as touch screens and displays, on a daily basis. These devices contain a common component - TCC, which can be used, for example, as a transparent counter electrode in a liquid crystal display (LCD). In a typical LCD device, the liquid crystals are aligned under an electrical potential generated between two electrodes, and in order to see the colors, one of the electrodes must be transparent. Another application of TCC is in touch screen devices, which are generally divided into a resistive and a capacitive types.<sup>1</sup> Furthermore, TCCs are used as electromagnetic shielding layers which prevent electromagnetic interference (EMI). This can be achieved by using materials with high conductivity, such as metals or conductive polymers, as a shielding package, yet allowing light transmittance.<sup>2,3</sup>

Various electronic and optoelectronic devices have a similar structure, where the TCC is one of the upper layers. Nowadays, the most common materials used for the fabrication of TCCs are metal oxides, while the most widely used oxide being indium tin oxide (ITO), with a market share of more than 97% of transparent conducting coatings.<sup>4</sup> ITO coatings are characterized by low sheet resistance, down to 10  $\Omega/\square$ , at about 90% optical transparency in the visible range.<sup>5</sup> However, ITO has several disadvantages, such as high production cost, the need for special etching processes in order to achieve patterning, and the need of the relatively rare element, indium. Another disadvantage is the brittleness of ITO thin films which prevents its utilization for the fabrication of flexible, stretchable, and bendable devices.<sup>4, 5</sup> Therefore, much effort is being made nowadays to find alternatives for ITO, which are based on nanomaterials, and which can be printed directly on various substrates. An ideal replacement should be a low cost material that would enable to obtain flexible thin transparent films by simple and low cost processes, including direct patterning. Depending on the application, the TCC replacement should have a sheet resistance in the range of 10 to 10<sup>3</sup>  $\Omega/\square$  at a transparency  $\geq 90\%$ .<sup>6,7</sup>

The emerging materials for ITO replacement can be divided into three categories: carbon based materials, such as carbon nanotubes (CNTs) and graphenes; metallic nanoparticles (NPs) and nanowires (NWs); and conductive polymers, such as

PEDOT:PSS.<sup>8</sup> In this review we will focus on the use of **conductive nanomaterials**, such as metallic NPs, metallic NWs, CNTs and graphene nanosheets for the fabrication of TCCs.

## 2. Metallic nanomaterials

Depending on the application, TCCs based on metallic nanomaterials, such as nanowires and grids, should possess sheet resistance in the range of 10 to 10<sup>3</sup>  $\Omega/\square$  at a transparency of  $\geq 90\%$ . 400-1000  $\Omega/\square$  is sufficient for many touch screen applications, and  $\sim 10$ -50  $\Omega/\square$  is required for OLEDs and solar cells.<sup>6,7</sup> The degree of transparency and conductivity can be tuned by varying the coverage of the surface, e.g. density of the deposited nanomaterial. While fabricating and patterning TCCs on plastic substrates for use in flexible plastic electronics, the main requirements are low-temperature processing, low-temperature post-patterning sintering ( $\leq 150$ -200  $^{\circ}\text{C}$ ) and strong adhesion of the metallic nanomaterials to the flexible substrates.<sup>9-13</sup>

### 2.1 Metal nanowires

Metal NWs can be defined as nano-sized rods with a high length-to-diameter aspect ratio, typically larger than 20. The most common metal NWs are made of silver. A typical method to synthesize silver NWs is by reducing the silver nitrate in presence of PVP, in ethylene glycol as reaction medium and reducer.<sup>14, 15</sup> Various solution-based methods are suitable for the production of TCCs which are composed of such metal NWs: drop casting,<sup>16</sup> spray-coating,<sup>17</sup> rod-coating,<sup>18</sup> spin-coating,<sup>19</sup> thermal nanoimprint lithography,<sup>20</sup> and vacuum filtration followed by transfer printing onto a proper substrate.<sup>21</sup> Due to the low intrinsic electrical resistivity of silver, the sheet resistance of films that can be obtained by using silver NWs is low, usually in the range of 10-100  $\Omega/\square$ , making it more favorable over carbon based TCCs.<sup>17, 22</sup> The films made of metallic NWs actually contain many voids in between them. The contacts between the individual wires provide the percolation paths to enable low conductivity, while the nanometric diameter of each NW leads to high transparency.

There are few reports, which describe theoretically<sup>23, 24</sup> and experimentally<sup>18, 21, 24</sup> the main parameters that govern the transparency and sheet resistance of the films. Mutiso *et al*<sup>23</sup>

presented a method that enabled computing of sheet resistance and empirical expressions for optical transparency, thus providing the first fully calculated plots of % T versus  $R_s$ . The model could predict the effect of the NW aspect ratio (length to diameter) and network morphology (areal density, dispersion, orientation, etc.)<sup>5</sup> on network properties. In another research, networks of silver NWs with wire diameters in the range of 45–110 nm and a pitch of 500, 700 and 1000 nm, were evaluated. The optimal transparency (91%) was obtained for the NWs network that had thin wires and a small pitch. The sheet resistance was as low as 6.5  $\Omega/\square$  for the best conducting network. By combining measurements and simulations, four distinct physical phenomena were found to govern the transmission of light through the networks, all related to localized surface plasmon and surface plasmon polaritons.<sup>24</sup>

A novel approach to increase the conductivity of NW-based TCCs is based on improving the interconnection between the NWs.<sup>25</sup> It has been shown that gold-decorated, reduced graphene oxide nano-platelets can bridge the closely located, non-contacting metal NWs. This can act as a protective and adhesive layer for the underneath metal NWs, which resulted in better performance of the TCC, compared to the untreated NWs. Interestingly, this hybrid TCC possesses antibacterial properties.

A simple approach for obtaining TCCs by using silver NWs is based on vacuum filtration of NWs dispersion, followed by transferring the NW film onto a PET substrate by heating and applying pressure.<sup>21</sup> The obtained TCC showed sheet resistance in the range of 1–100  $\Omega/\square$ , depending on coating density. Recently, better results (sheet resistance <1  $\Omega/\square$  at 92% transparency) were reported for films that have been obtained by combining mesoscale metal with the NWs.<sup>26</sup> An additional layer of copper mesoscale wires (1–5  $\mu\text{m}$ ) was deposited (Fig. 1) over a layer of NWs (50–300 nm in length). The optimal films, in view of conductivity and transparency, as was found by simulations, should be composed of wires with diameter of 5  $\mu\text{m}$  and spacing of 100–500  $\mu\text{m}$ .

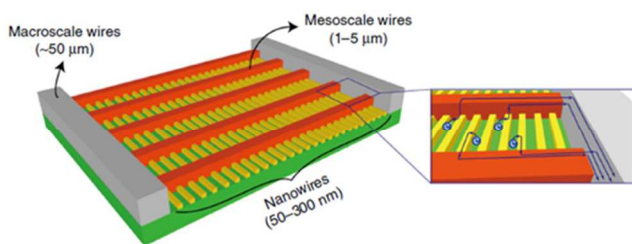


**Fig. 1** Mesoscale metal-wire network, TCE concept. Scheme of mesoscale design (not drawn to scale). The mesoscale metal-wire network between the nanowire transparent electrode and the macroscale wires (metal fingers), can shorten the distance of the carrier transport and enhance the  $R_s$ -T performance. Adapted with permission from Macmillan Publishers Ltd: Nature<sup>26</sup> copyrights 2013.

Increasing the conductivity of the NW film by using longer wires was also reported by Lee *et al.*<sup>27</sup> By combining a novel method of synthesis of very long Ag NWs (>500  $\mu\text{m}$ ) with low temperature, laser nano-welding process, highly transparent and flexible conductors with high transmittance (89–95%), high electrical conductivity (9–69  $\Omega/\square$ ), and good mechanical strength, were

obtained.<sup>27</sup> Fig. 2 shows the effect of NWs length on sheet resistance and transmittance.

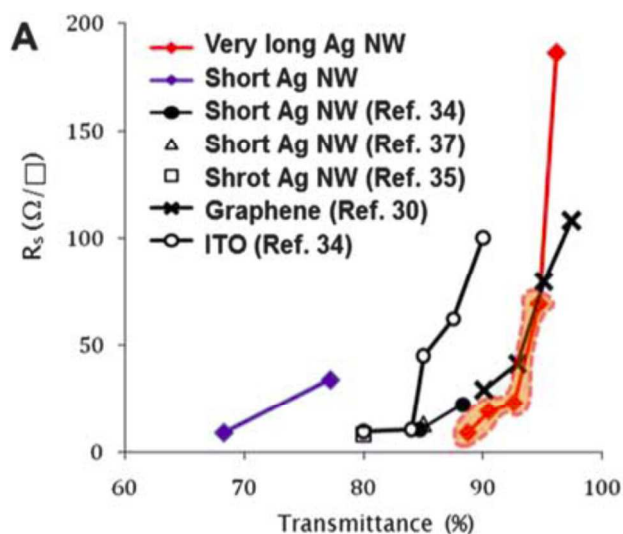


**Fig. 2** Optical and electrical characteristics of Ag NWs-based TCCs: plots of sheet resistance vs optical transmittance at 550 nm for networks of various NWs. Adapted from reference 27.

An interesting approach for obtaining TCCs based on *in situ* formation of NWs of two metals, was reported by Azulai *et al.*<sup>28</sup> Gold/silver nanowire meshes were formed after the reduction of the metal ions was triggered, followed by spreading a thin growth solution on the substrate. The reduction of the metal progressed within a template of a highly concentrated, surfactant liquid crystalline mesostructure, formed on the substrate during film drying, to form ordered bundles of ultrathin nanowires. Such films were grown on silicon, quartz and PET, and were characterized by sheet resistance in the range of 60–1000  $\Omega/\square$  and transmittance comparable to the transmittance of ITO films.<sup>28</sup> Although the most widely studied NWs are made of silver, copper NWs were also reported. Copper TCC films were formed by filtering aqueous dispersion of NWs (average length and diameter 10  $\mu\text{m}$  and 90 nm respectively) through polycarbonate membrane, followed by imprinting onto a glass slide. The obtained sheet resistance of such films was 15  $\Omega/\square$  with transmittance of 65% at 500 nm.<sup>29</sup> Another type of Cu NWs-based TCC was obtained by rod-coating a dispersion containing nitrocellulose as a film former. The obtained coatings were treated with  $\text{H}_2/\text{N}_2$  plasma and heated under  $\text{H}_2$  atmosphere at 175  $^\circ\text{C}$ . The resulting sheet resistance was 30–185  $\Omega/\square$  and the transmittance was 85–90%, depending on the density of the coating.<sup>29</sup>

Copper nanofibers (diameter:  $\sim$ 100 nm, length: >100  $\mu\text{m}$ ) were also used to produce TCC. The coating on a glass slide was performed by electrospinning, and resulted in sheet resistances of 200 and 50  $\Omega/\square$ , at transparencies of 96 and 90% (at 300–1100 nm), respectively.<sup>30</sup>

As was already mentioned regarding rigidity of ITO films, an important parameter for practical application of TCCs on flexible substrates is their stability towards bending. NWs have been shown to be a promising candidate due to the inherent mechanical stability of the individual NWs. For example, only  $\leq$ 2% increase

in sheet resistance of silver and copper NWS-based thin film on PET was observed, after 100-1000 cycles of bending,<sup>21</sup> as compared with 400-time increase of sheet resistance of ITO films, after only 250 bending cycles.<sup>19</sup> TCCs made of NWs have been reported for various applications, such as solar cells, and have already been incorporated in some optoelectronic devices.<sup>31</sup> Recently, it has been shown that a silver NWs layer can be applied for electromagnetic shielding.<sup>3</sup> The silver NWs were imbedded in between a PET substrate and a layer of transparent polyethersulfone (PES), to decrease the shedding and corrosion of silver NWs. Prior to the PES coating, the NWs were deposited onto PET in presence of polyethylene oxide (PEO), which provides a homogeneous distribution of the NWs layer. After thermal removal of the PEO at 160 °C, the formed "sandwich" film showed excellent EMI shielding performance. For films with >80% transmittance, the lowest sheet resistance was 14.7  $\Omega/\square$ , and the EMI shielding was ~30 dB, which is better than the minimum value of 20 dB required for commercial applications.<sup>3</sup> It should be noted that the performance of conductive polymer composites and carbon-based conductive films as EMI shielding, is usually lower.<sup>32-34</sup>

To the best of our knowledge, silver NWS-based TCCs are the only ones which have already been commercialized. Films with sheet resistance in the range of 10-300  $\Omega/\square$  ("ClearOhm" product) produced by Cambrios Technologies, have been successfully incorporated in touch screens and displays by LG Electronics (Korea), in large area monitors of eTurbotouch Technology (Taiwan), in mobile phones of NEC/NTT Docomo (Japan), and in kiosk monitors of G-Vision (USA).

## 2.2 Patterning of metal nanoparticles

Typically, most TCCs are achieved by using materials that possess intrinsic properties which enable transparency. This is true for metal oxides and carbon-based materials at low thickness. A major emerging concept for obtaining TCC which contain metal nanoparticles is by fabricating various patterns such as grids, arrays and honeycombs, with very narrow line features.

### 2.2.1 Grids

TCCs formed by a grid patterns are becoming commercially available. Among the many companies that are utilizing this approach are: POLYIC, Toray and Rolith. Typical technologies to achieve conductive transparent metal grids are based on photolithography<sup>35-37</sup> direct printing,<sup>9, 38</sup> embossing,<sup>39</sup> and self assembly.<sup>40</sup> All these methods enable obtaining narrow lines (<10  $\mu\text{m}$ ) and low sheet resistance (<10  $\Omega/\square$ ) of the whole grid.

While performing the patterning process with metallic NPs (such as in a printing process) a very important step for achieving conductive patterns (not necessarily transparent) is required, the sintering of the metallic particles to enable percolation path for electrical conductivity. In order to obtain a stable dispersion of metal NPs (where the NPs do not aggregate or sediment over time), organic stabilizing agents are usually used (polymers or surfactants). The molecules of such insulating stabilizing agents are adsorbed at the surface of the NPs, but they should be removed after formation of forming the metallic films, in order to obtain tightly packed, conductive layers with numerous interconnections. Therefore, a very important step in obtaining NPs-based TCCs is the sintering, which is a process of merging

the particles without their complete melting. There are various approaches to sinter metal NPs: thermal,<sup>40</sup> chemical<sup>40</sup> and plasma<sup>60</sup> sintering<sup>42</sup>, sintering under microwave radiation<sup>43</sup>, light flashing<sup>44</sup>, electrical<sup>45</sup> and laser sintering.<sup>46</sup> It should be noted that thermal sintering is usually performed at temperatures above 200°C, which is not suitable for plastic substrates, and therefore non-destructive methods of sintering, such as, for example, light flashing, are preferable.<sup>47</sup>

Obviously, in case of thermal sintering, local heating can be utilized for both sintering and forming the grid. For example, a top-down approach to obtain a transparent conductive grid (TCG) by selective laser sintering was recently reported.<sup>47, 48</sup> By this process (Fig. 3), the heat generated by the laser causes sintering of the particles within predetermined narrow lines with required shapes. The patterning process is followed by washing out the remaining unsintered particles, and a transparent conductive grid is obtained. The transparency and conductivity can be controlled by varying the dimensions of the grid and the width of the lines. For grids composed of 300x300  $\mu\text{m}$  squares with 10-15  $\mu\text{m}$  line width, a TCC with sheet resistances of <30  $\Omega/\square$  and 85% transparency was obtained. It is interesting to note that while using laser sintering with short pulse time, it is possible to produce the TCG without destroying the plastic substrates.<sup>47</sup>

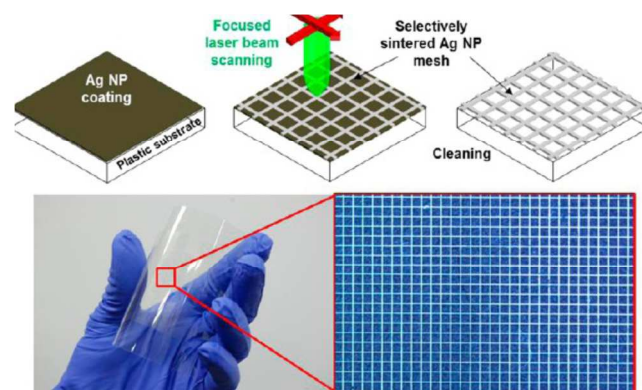


**Fig. 3** Schematic diagram of selective laser sintering of Ag NPs for the fabrication of a transparent conductor. Bottom part, transparent conductor fabricated on a flexible (PEN) substrate (metallic grid on a 5x5 cm region). Adapted with permission from S. Hong, J. Yeo, G. Kim, D. Kim, H. Lee, J. Kwon, H. Lee, P. Lee and S. H. Ko, *ACS Nano*, 2013, 7, 5024-5031. Copyright 2013 American Chemical Society.<sup>47</sup>

The main disadvantage of this approach is the large amount of un-sintered, costly material which should be removed after the grid formation sintering.

Ahn *et al*<sup>10</sup> used a direct patterning of concentrated ink containing silver NPs (>70 wt%), by extrusion through a very narrow cylindrical nozzle. The printed feature's dimensions are determined by the ink rheology and printing parameters, with a typical line width of ~5  $\mu\text{m}$ , a height of 280 nm and center-to-center spacing of 100-400  $\mu\text{m}$ , as shown in Fig. 4. The best transparency, ~94%, was obtained for 400  $\mu\text{m}$  spacing. The resistivity was  $3.64 \times 10^{-5} \Omega\text{-cm}$  after annealing at 200 to 350 °C for 2 hours<sup>10</sup>.

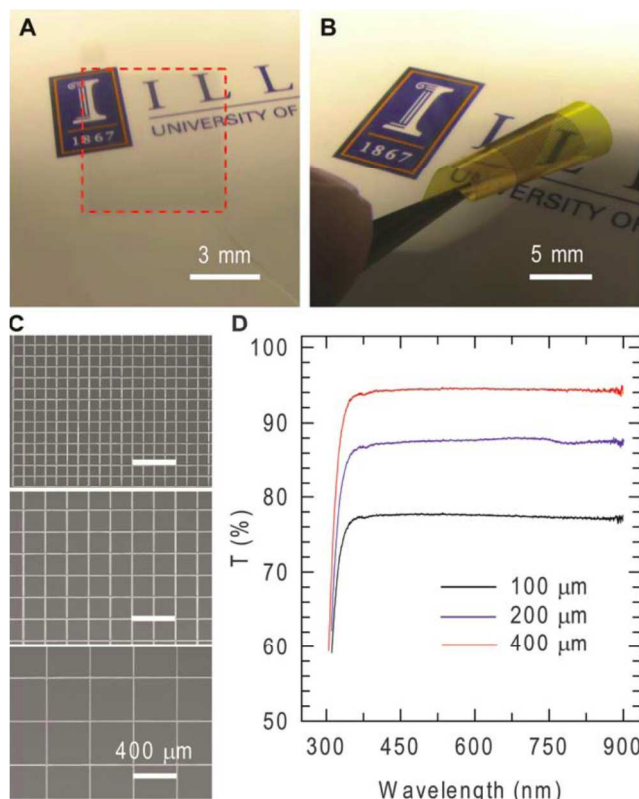


**Fig. 4** Optical images of the TCGs with center-to-center line spacing of 200  $\mu\text{m}$ , printed on (A) glass and (B) polyimide substrates. (C) SEM micrographs of the conductive grids, printed with center-to-center spacing of 100  $\mu\text{m}$  (top), 200  $\mu\text{m}$  (middle), and 400  $\mu\text{m}$ , respectively. (D) Transmittance of the conductive grids of varying center-to-center spacing patterned on glass substrates. Adapted from reference 10.

Nanoimprinting is another method for obtaining semi-transparent grids<sup>37</sup>, which utilizes imprinting molds fabricated by photolithography, as presented in Fig. 5. The transparency and sheet resistance can be controlled by changing the metal type and layer thickness. For example, for layer thickness of 80 nm, all metals (Au, Cu and Al) yielded sheet resistance of  $\sim 5 \Omega/\square$  at 70% transparency, while Cu and Au layers of 40 nm thickness, were characterized by sheet resistance of  $\sim 15 \Omega/\square$  and  $11 \Omega/\square$ , respectively<sup>37</sup>, at 70% transparency.

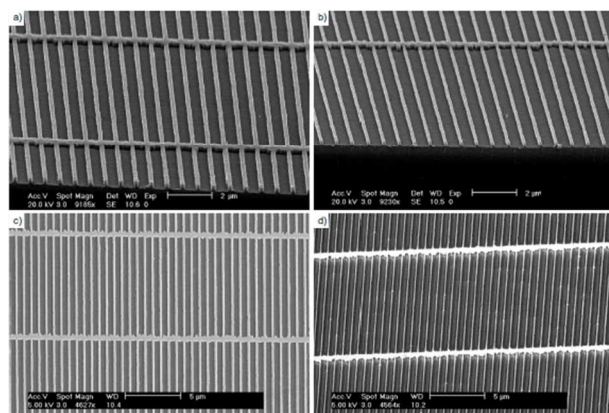


**Fig. 5** SEM images of imprinting molds with rectangular grids with line widths of (a) 200 nm and (b) 120 nm, and the corresponding semi-transparent metal electrodes (on glass) with line widths of (c) 200 nm

and (d) 120 nm. Data reproduced with permission of WILEY-VCH Verlag GmbH & Co.<sup>37</sup>

A very recent approach for the production of TCGs is by combining inkjet printing and coffee stain effect<sup>38, 49-51</sup>. The coffee stain effect is a process in which particles within a sessile drop move towards the periphery of the drop during evaporation. Upon evaporation, the outer parts of the ring are composed of closely packed particles. As will be described later, based on this effect, a transparent conductive layer can be formed, composed of multiple interconnected rings.<sup>49</sup> Zhang et al.<sup>38</sup> recently reported on the formation of elongated ellipse-shaped patterns based on this effect, while the nanoparticles are accumulated in narrow parts of printed lines. The width of the line composed of silver NPs was 5-10  $\mu\text{m}$  that resulted in a transparent pattern (Fig. 6). These ellipse shaped patterns were interconnected in the form of a grid. The resulting TCG on glass had a transparency of 92% with line resistivity in the range of  $2.61 \times 10^{-3} - 5.76 \times 10^{-4} \Omega\text{-cm}$  when annealed at 160–200  $^{\circ}\text{C}$  for 2 hours.<sup>38</sup>

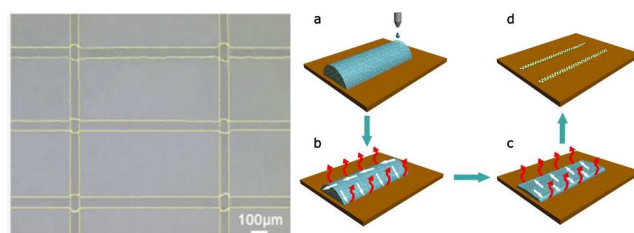


**Fig. 6** Left: Optical image of a reticular conductive pattern based on printed coffee-ring lines of Ag NPs. Right: Schematic illustration of inkjet printing of Ag-NPs patterns induced by the coffee-ring effect. (a) A single line is fabricated by ink-jet printing of Ag NPs ink on the substrate. (b, c) The Ag NPs migrate to the TCL during the solvent evaporation. (d) The final deposited Ag NPs patterns. Data reproduced with permission of WILEY-VCH Verlag GmbH & Co.<sup>38</sup>

A different approach, which is also derived from wetting and self assembly processes, was presented by Higashitani et al.,<sup>52</sup> who produced a gold TCG using an evaporative lithography method. First, a stainless-steel mesh was placed on top of a glass substrate. Next, a droplet containing gold NPs was placed on top of the mesh, instantaneously spreading over the mesh and the glass substrate. During evaporation, the liquid flowed towards the metal wires of the mesh, leaving an empty area under every one of its squares. After complete evaporation, the mesh was removed from the glass substrate, and a transparent grid composed of the gold NPs was obtained. At this stage, the gold grid was not conductive, probably due to the presence of a polymeric stabilizer around the nanoparticles. Hence, a thermal sintering was conducted (425  $^{\circ}\text{C}$  for 20 min). Then the conductive network was transferred onto a polymeric film by pressing it into a thin layer of UV hardening resin coated on a PET film. In the final step of the process UV curing was performed, yielding a metallic grid on a plastic substrate.

Obviously, the need to sinter the particles at high temperatures prevents the possibility of obtaining a transparent grid directly on a plastic substrate, and requires a complex transfer process of the grid from the glass to a soft film forming material. Layani *et al.*<sup>53</sup> used a similar evaporative lithography method, but it was performed directly on a PET substrate. The sintering was

performed at low temperature, by a simple chemical sintering process. This process resulted in TCG with a sheet resistance of  $\sim 9 \Omega/\square$  and  $\sim 80\%$  transparency.

One of the challenges of such transparent grids is that their conductive layer is not continuous and contains voids which are not conductive. In order to turn the TCG into a fully and continuous conductive layer, the voids should be filled with an additional transparent conductive material, for example, conductive polymer PEDOT:PSS. Zou *et al.*<sup>35</sup> used PDMS stamping to fabricate silver grids with line width of 5, 10 and 20  $\mu\text{m}$ , with line separation of 50, 100, 200  $\mu\text{m}$ , respectively, followed by coating with a layer of PEDOT:PSS. These coated grids were then used in inverted polymeric solar cells as transparent electrodes (structure presented in Fig. 7). When comparing uncoated grids with coated grids of the same dimensions, the efficiencies of the solar cell composed of coated grids were almost 3 times higher.<sup>35</sup>

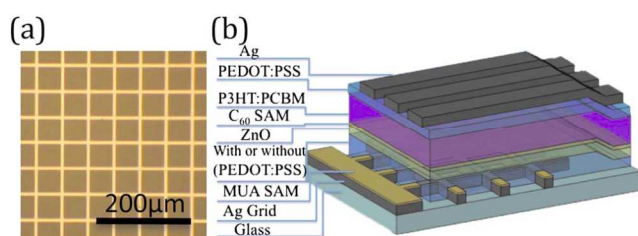


**Fig. 7** (a) Optical microscope image of silver grid with 5  $\mu\text{m}$  width separated by a distance of 50  $\mu\text{m}$ . (b) Device configuration of the polymer solar cell using Ag grid as the transparent electrode with or without conductive PEDOT:PSS layer. Reproduced with permission from AIP Publishing LLC.<sup>35</sup>

Another material that was used to fill in the voids is graphene,<sup>36</sup> as schematically shown in Fig. 8. The sheet resistance of the resulting hybrid transparent electrodes was as low as  $3 \Omega/\square$  with transmittance of  $\sim 80\%$ , and  $\sim 20 \Omega/\square$  for films with 90% transmittance. Due to the intrinsic properties of graphene, the light absorbed by such thin layers is only 2.3% of the incident light. The metal grid in this study was fabricated by photolithography of thin sputtered layers of Cu, Au, or Al, while graphene was deposited on top of the grid by either CVD or low temperature growth techniques.<sup>36</sup>

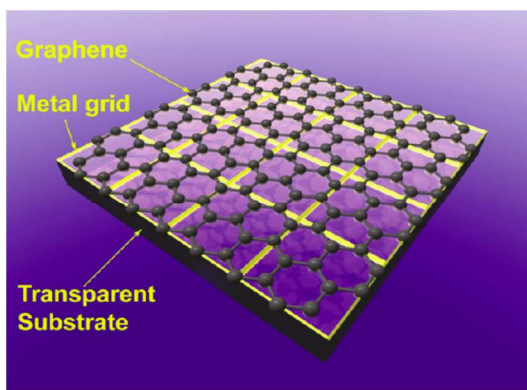


**Fig. 8** Metal grid/graphene hybrid transparent electrode. The yellow lines in the figure represent the metal grid. The grid size and gridline width in the figure are only illustrative and are not scaled with the graphene molecular structure. Reprinted with permission from Y. Zhu, Z.

Z. Sun, Z. Yan, Z. Jin and J. M. Tour, *ACS Nano*, 2011, 5, 7686-7686. Copyrights 2013 American Chemical Society.<sup>36</sup>

### 2.2.2 Honeycomb structure

As mentioned earlier, when using nanomaterials to pattern a transparent electrode, it is highly important that the morphology of the conductive pattern provides high transparency. Therefore, it is also important to find the pattern that will not reduce the charge collection over the whole layer. For example, in the previously described TCG, the size of the squares (non-conductive voids) should be tailored according to the electrical requirements of the device, so that the voids within the grid should not be too large. Obviously, decreasing the voids' dimensions will cause a reduction in transparency. Another way to optimize the charge collection is to change the geometry of the conductive lines from a grid pattern to a honeycomb structure (Fig. 9). For example, Galagan *et al.*<sup>54, 55</sup> printed current collecting grid in a honeycomb structure combined with solution-processed conductive PEDOT:PSS. The semi-transparent honeycomb grids were screen printed using a commercial nano-silver paste (TEC-PA-010, Inktec). The active area of the TCC was 2x2 cm with a line width of 160  $\mu\text{m}$ , and a sheet resistance of  $1 \Omega/\square$ . This TCC was integrated in an organic solar cell as the anode. The efficiency of the device with an active area of 4  $\text{cm}^2$  was about two times higher than that of a device with ITO as the transparent electrode.

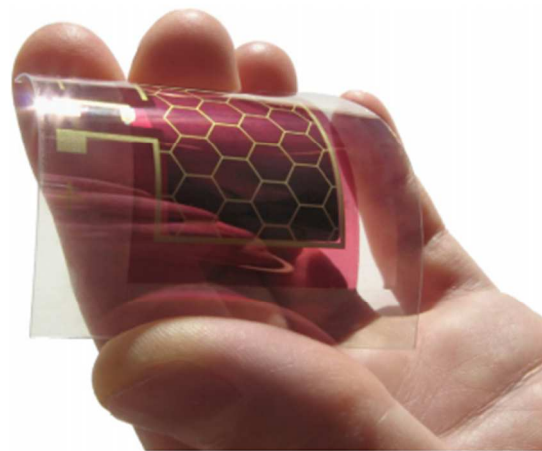


**Fig. 9** A 2x2 cm solar cell with current collecting grid, free of ITO. Reproduced with permission from Elsevier.<sup>55</sup>

A nanometric honeycomb structure can be obtained by combining self-assembly and nano-sphere lithography.<sup>56</sup> The process involves three main steps. First, polystyrene (PS) spheres are arranged on a substrate to form a monolayer or multilayer template. This can be done by various methods, such as Langmuir-Blodgett films, spin coating, dip deposition or floating-transferring techniques. Next, the voids among the PS spheres are filled with the required materials. Finally, the PS sphere template is removed, leaving behind a nanostructured pattern on the substrate.<sup>57, 58</sup> To fabricate a gold honeycomb structure, once the PS monolayer is obtained, a gold layer is formed on top of the spheres by thermal evaporation in vacuum, and the PS template is removed by rinsing with tetrahydrofuran.

The voids between the PS spheres were expanded by reactive ion etching, in order to obtain better continuity and electrical conductivity of the metal network. The effect of the etching time on the optical and electrical properties was evaluated.<sup>58</sup> To construct a honeycomb structure composed of silver NPs (Fig. 5 10), a droplet of silver ink was placed onto the monolayer of PS spheres. The silver NPs were thermally sintered, followed by removal of the PS monolayer by sonication in toluene. The resulting TCC had a transmittance and sheet resistance of 83% and 20  $\Omega/\square$ , 10 respectively.<sup>57</sup>

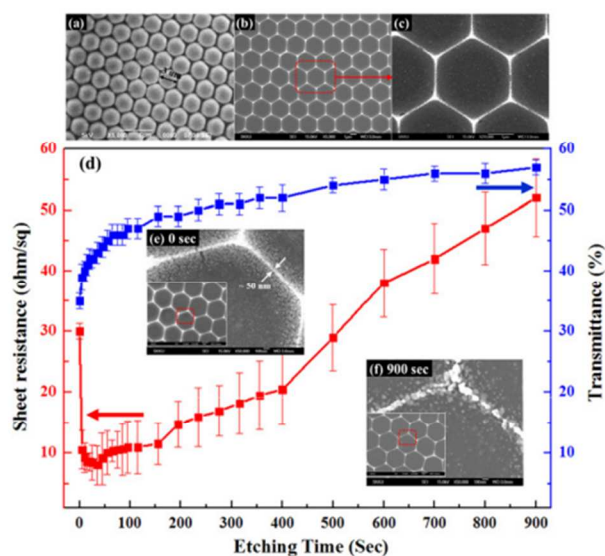


**Fig. 10** FE-SEM images of (a) a 3  $\mu\text{m}$  PS sphere monolayer and (b) an Ag honeycomb mesh. (c) Enlargement of the dotted box in (b). (d) Variation in sheet resistance and transmittance of Ag honeycomb mesh constructed by using 3  $\mu\text{m}$  PS with etching time and (f) FE-SEM images of Ag honeycomb mesh before and after etching for 900 s, respectively. © IOP Publishing. Reproduced by permission of IOP Publishing.<sup>57</sup>

### 2.2.3 Rings

TCC can be fabricated by printing multiple interconnected rings, by the coffee stain effect.<sup>49</sup> Each printed ink droplet (by inkjet printing) form an individual ring composed of closely packed metallic nanoparticles. At proper printing conditions, many rings can be printed and connected spontaneously, and if sintered, the formed transparent array of rings is also conductive.

More specifically, the conductive arrays were obtained by ink-jet printing of picoliter droplets of a silver dispersion directly onto a flexible substrate. After printing, each printed dot is self-assembled into a ring by the well-known "coffee ring effect".<sup>59</sup> As reported by Deegan et al.,<sup>59</sup> once a millimeter-size droplet of liquid containing solid particles is pinned to a substrate, upon drying of the droplet, the solid particles assemble into a ring. Such effect is usually undesirable since the typical high quality ink-jet printed pattern is uniform.<sup>60, 61</sup> As shown by Perelaer et al.<sup>62</sup> and Kamyshny et al.,<sup>51</sup> micrometric individual rings can be obtained by ink-jet printing of dispersions of silica particles or microemulsion droplets, respectively.

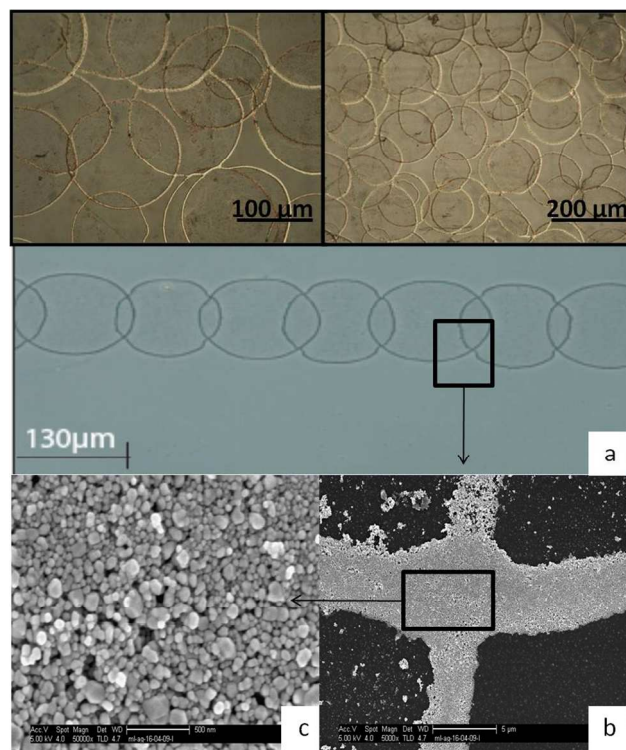


**Fig. 11** Upper image: array of interconnected rings. (a) Light microscope image of a chain of rings. (b and c) SEM images showing a closer look at the junction between two rings. Reprinted with permission from M. Layani, M. Gruchko, O. Milo, I. Balberg, D. Azulay and S. Magdassi, *ACS Nano*, 2009, 3, 3537-3542. Copyrights 2013 American Chemical Society.<sup>49</sup>

In our previous report,<sup>50</sup> we have shown that in the case of dispersions of metallic NPs, this "coffee stain" effect can lead to the formation of conductive, millimeter size rings without the need for sintering at high temperatures, due to the spontaneous close packing of the silver NPs at the rim of the ring. In continuation of these findings, we utilized the coffee ring effect to obtain 2D arrays composed of interconnected conductive rings which possess high transparency and conductivity. Arrays of silver rings were obtained by ink-jet printing of ink composed of silver NPs, directly onto plastic substrate (Fig. 11), yielding a TCC with 95% transparency and sheet resistance of  $4 \pm 0.5 \Omega/\square$ .<sup>49</sup> This type of 2D ring array enabled the fabrication of a flexible, plastic electroluminescent device, in which the array which is directly printed on a PET film and sintered at low temperature, serves as transparent conductive which replaces the typically used ITO in such devices.

Fabricating a TCC as a 2D ring array may have several additional advantages. Simulations show that at the same periodicity and line width, ring mesh has better transmissivity in the visible range because of its higher obscuration ratio, stronger electromagnetic shielding performance due to smaller maximum aperture, and less degradation of imaging quality because of lower ratio and uniform distribution of high order diffraction.<sup>63</sup> Nevertheless, to the best of our knowledge, there is only one report on the fabrication of a TCC as a ring array pattern.<sup>49</sup>

## 3 Carbon based nanomaterials

### 3.1 Graphene

Graphene is the most recently discovered allotrope of carbon.<sup>64</sup> A typical graphene flake has a width of up to 50  $\mu\text{m}$  and thickness of 0.34 nm.<sup>65</sup> It is characterized by very high Fermi velocity (106 m/s) and high intrinsic in-plane conductivity.<sup>7, 66</sup> As predicted, the sheet resistance of graphene TCC varies with the number of layers,  $N$ , as  $R_s \sim 62.4/N \Omega/\square$ .<sup>67</sup>

Graphene and its derivatives are produced by several methods: from graphite by mechanical<sup>65</sup> and liquid phase<sup>68, 69</sup> exfoliation, by chemical vapor deposition (CVD),<sup>69, 70</sup> by synthesis from various organic compounds,<sup>71</sup> by chemical cross-linking of polycyclic aromatic hydrocarbons,<sup>71</sup> and by thermal decomposition of SiC.<sup>72</sup> The most often used nanomaterial for the formation of graphene coatings is graphene oxide (GO), because of its good dispersibility in water and its high electrical conductivity, which can be achieved by a reduction process after forming the coating by wet deposition. The latter can be performed by chemical or thermal treatment.<sup>73</sup> GO is usually obtained by oxidation of graphite powder in presence of strong acids and oxidants.<sup>73, 74</sup>

There are several reports on the production of TCCs using graphenes.<sup>69, 74-77</sup> The typical sheet resistance of a graphene-based TCCs is in the range of 200-1000  $\Omega/\square$  with transparency lower than 90%.<sup>74, 78</sup> Improving the sheet resistance of graphene can be achieved by increasing the number of graphene sheet layers,<sup>79</sup> but obviously, this would cause a decrease in transparency.

A recent report by Yuan et al.<sup>80</sup> showed how tailoring of the electrical and optical properties can be performed by exposing the graphene TCC to ozone for various time periods at various temperatures. Initially, ozone exposure dramatically decreases the electrical resistance of the graphene films by p-doping, but this is followed by increase in the resistance and optical transmittance as a result of surface oxidation. The rate of resistance increase can be significantly increased by raising the treatment temperature. By this approach, the sheet resistance decreased from 1300 to 320  $\Omega/\square$  at 20 °C after 60 sec exposure.<sup>80</sup> To date, the best reported graphene-based TCC has a sheet resistance of 8.8  $\Omega/\square$ , at 84% transparency.<sup>81</sup> These graphene films were obtained by intercalating few-layer graphene with ferric chloride. It should be noted that graphene-based materials offer good electromagnetic shielding<sup>82-84</sup> and might be a good candidate for EMI shielding TCCs.

### 3.2 Carbon nanotubes

CNTs are formed by folding a graphene sheets into a cylindrical hollow structure, in which the walls are constructed by carbon atoms. The graphene sheets can differ in their chirality, and depending on that, the CNT can have either a semiconductor or metallic properties. They can be both as single-walled CNTs (SWCNTs) and as multi-walled CNTs (MWCNTs), and have a typical length of several to tens of microns. The diameter of SWCNTs is usually in the range of 0.4-4 nm, while the outer diameter of MWCNTs is in the range of several to tens of nanometers.<sup>85</sup>

The electrical resistivity of an individual CNT can be as low as  $1 \cdot 10^{-6} \Omega\text{-cm}$  for SWCNT<sup>84</sup> and  $3 \cdot 10^{-5} \Omega\text{-cm}$  for MWCNT.<sup>86</sup> However, in most cases, due to the presence of various defects or impurities, the resistivities of individual CNTs, as well as the resistivities of their assemblies, are much higher.<sup>87</sup> Due to the superior mechanical properties of individual CNTs,<sup>88</sup>

thin films made of CNTs are promising candidates for the production of flexible electronic devices. There are three major methods for the production of CNTs: electric arc discharge, laser ablation, and chemical vapor deposition (CVD).<sup>89-91</sup> The arc discharge method usually requires high temperatures (above 1700 °C). Although the most often used method is DC discharge between two graphite water-cooled electrodes with helium at sub-atmospheric pressure, hydrogen and methane gases are also used.<sup>91</sup> CNTs are attracted to the cathode, while the anode is consumed. Usually MWCNTs are produced by this method, if no catalyst is used. On the other hand, the method used to produce SWCNTs normally requires a metal catalyst (Fe, Ni, Co, Mo, Y).<sup>91</sup> If high quality and purity SWCNTs are desired, laser-induced evaporation/ablation of pure graphite (by Nd:YAG or CO<sub>2</sub> lasers) is used.<sup>91</sup> Catalytic CVD, thermal or plasma enhanced, which is the catalytic decomposition of hydrocarbons or carbon monoxide, is also a common method for obtaining high purity CNTs. It was previously shown that CNTs can also be fabricated by flame pyrolysis, using carbon monoxide as a carbon source.<sup>92</sup> An organic synthesis method was also demonstrated to form homogeneous CNTs with well defined structures. The synthesis is performed by utilizing hoop-shaped carbon macrocycles (small fragments of CNTs that retain information regarding chirality and diameter), which are used as templates for polymerization reactions to produce long CNTs.<sup>93</sup> Another bottom-up approach to produce MWCNTs is the hydrothermal processing of a mixtures of polyethylene and water, or ethylene glycol and water with an Ni catalyst at 700-800 °C, under pressure of 60-100 MPa,<sup>94</sup> and by the electrolytic process, which involves graphite cathode immersed in molten chlorides of alkali, or alkaline-earth metals.<sup>90</sup>

There are various methods that can be used for the preparation of CNT transparent films by wet deposition: rod-coating,<sup>95</sup> spin-coating,<sup>96</sup> spray-coating,<sup>97</sup> dip-coating,<sup>98</sup> drop-casting,<sup>99</sup> vacuum filtration followed by transfer onto a proper substrate,<sup>100</sup> electrophoretic deposition followed by hot pressing transfer,<sup>101</sup> and inkjet printing.<sup>102, 103</sup> The best approach to increase the conductivity of the film, is by stacking more and more CNT layers. However, increasing the amount of material will lead to a decrease in transparency. CNT films with a transparency suitable for most electronic applications have a typical thickness of  $\leq 50 \text{ nm}$ .<sup>7</sup> Since SWCNTs have higher conductivity compared to MWCNTs, they are preferable for the fabrication of conductive transparent films. Typical sheet resistance and transparency of such films, on glass and plastic substrates, are usually in the range of 60-870  $\Omega/\square$  and 70-90% (usually measured at 550 nm), respectively, depending on the film thickness and method of preparation.<sup>99, 102</sup> For example, deposition of CNTs onto PET from chlorosulfonic superacid resulted in TCC sheet resistance of 60  $\Omega/\square$  with a 90.9% transmittance.<sup>100</sup> Even lower sheet resistance, 4-24  $\Omega/\square$ , for hybrid films with up to 82% transparency, was recently reported.<sup>104</sup> This result was achieved by combining silver NWs with CNTs. The hybrid film was prepared by performing vacuum filtration through a cellulose ester membrane of a mixed dispersion of Ag NWs and SWCNTs, followed by transferring the film to a glass substrate. It was shown that the SWCNTs wrapped the Ag NWs, resulting in a conductive interconnect, as well as a mechanical support,

providing structural integrity of the films.<sup>104</sup>

Application of the CNT-based TCCs in solar cells and touch screens was already reported.<sup>105-107</sup> For example, low roughness SWNT films were fabricated by combining dip-coating with nitric acid treatment. These TCCs were then incorporated as an anode in an organic solar cell. The metallic-enriched SWNT anodes are found to yield power conversion efficiency that is 50 times greater than that for semiconducting SWNT anodes. It has been found that for the SWCNT-based organic photovoltaic (OPV) cells, the efficiency was ~2% compared to 3.1% for ITO-based OPV.<sup>106</sup>

CNT films on plastic substrates were also incorporated as the touch electrode in a four-wire resistive touch panel. Single-point actuation tests showed superior mechanical performance compared to ITO touch electrodes, with no loss of device functionality up to 3 million actuations. Sliding stylus-pen tests showed no loss of device linearity after 1 million stylus cycles. The CNT films on PET gave an 86% total transmission (including the PET) over the visible range and 600  $\Omega/\square$  sheet resistance.<sup>107</sup>

In addition, there are several reports showing that CNTs and carbon nanofibers (CNF) can serve as good transparent EMI shielders.<sup>34, 108</sup> For example, for a composite 40 wt% MWCNT/PMMA, the EMI shielding was 27 dB.<sup>33</sup> A very recent study showed that EMI shielding was 25 dB when using (CNF)-reinforced syntactic foam (CNFRSF) as the functional layer,<sup>34</sup> which is better than 20 dB as the minimum value typically required for commercial applications.<sup>3</sup>

It should be mentioned that CNTs can form both non-transparent electrodes and a TCC, depending on the amount of CNTs and the film thickness. Therefore, we fabricated recently a flexible, plastic electroluminescent device, in which the transparent back electrode was formed by spray coating of a CNT dispersion, and the counter electrode was patterned by inkjet printing a CNT dispersion.<sup>108</sup>

Currently, only very few commercial CNT films are available as competitors for ITO,<sup>4</sup> but more can be expected in the near future, since there are many research activities on this subject.

## 4 Outlook

As follows from the above overview, a number of nanomaterials of various chemical origins (metals, carbon) and morphologies (NPs, NWs, nanosheets, nanotubes) can be utilized for the fabrication of TCCs. In spite of the remarkable scientific progress in preparation processes and applications of conductive nanomaterials, they are still not widely used in the industry.

We expect that replacing the traditional metal oxides (mainly ITO), which are used as transparent electrodes in many displays, by TCCs made of conductive nanomaterials (metals, CNTs, and graphene), can make a revolutionary impact on modern optoelectronics. Among the transparent conductive coatings, currently the metal NWs-based TCCs are probably the most mature. CNT-based TCCs are also available commercially, and we expect that graphene will play a more significant role once suitable wet deposition methods will be developed. Furthermore, we also expect that, combining several types of methods and materials would result in efficient hybrid TCCs with superior properties.

## Acknowledgment

We acknowledge the support of Singapore National Research Foundation under the Campus for Research Excellence And Technological Enterprise (CREATE) programme: Nanomaterials for Energy and Water Management, NRF2009EWT-CERP001-026, and Israel Nanoscience and Nanotechnology Initiative, programme: FTA.

## Notes and references

*Institute of Chemistry, Casali center for applied chemistry and the Center for Nanoscience and Nanotechnology, The Hebrew University of Jerusalem, Jerusalem, 91904, Israel; E-mail: magdassi@mail.huji.ac.il*

1. <http://www.eizo.com>
2. H. C. Lee, J. Y. Kim, C. H. Noh, K. Y. Song and S. H. Cho, *Appl Surf Sci*, 2006, **252**, 2665-2672.
3. M. J. Hu, J. F. Gao, Y. C. Dong, K. Li, G. C. Shan, S. L. Yang and R. K. Y. Li, *Langmuir*, 2012, **28**, 7101-7106.
4. C. M. Niu, *Mrs Bull*, 2011, **36**, 766-773.
5. S. Park, M. Vosguerichian and Z. A. Bao, *Nanoscale*, 2013, **5**, 1727-1752.
6. L. B. Hu, H. Wu and Y. Cui, *Mrs Bull*, 2011, **36**, 760-765.
7. D. S. Hecht, L. B. Hu and G. Irvin, *Adv Mater*, 2011, **23**, 1482-1513.
8. H. Yan and H. Okuzaki, *Macromolecular symposia*, 2010, **296**, 286-293.
9. J. S. Yu, J. Jo, S. M. Yoon and D. J. Kim, *J Nanosci Nanotechnol*, 2012, **12**, 1179-1182.
10. B. Y. Ahn, D. J. Lorang and J. A. Lewis, *Nanoscale*, 2011, **3**, 2700-2702.
11. A. a. M. Kamyshny, S., *Small*, 2014.
12. A. Kim, Won, Y., Woo, K., Jeong, S. and Moon, J., *Adv Funct Mater*, 2014.
13. D. D. Y. Jin, and F. Xiao, *Electronic Components and Technology Conference*, 2013, 1315-1319.
14. B. Wiley, Y. G. Sun, B. Mayers and Y. N. Xia, *Chem-Eur J*, 2005, **11**, 454-463.
15. Y. G. Sun and Y. N. Xia, *Adv Mater*, 2002, **14**, 833-837.
16. J. Y. Lee, S. T. Connor, Y. Cui and P. Peumans, *Nano Lett*, 2008, **8**, 689-692.
17. A. R. Madaria, A. Kumar and C. W. Zhou, *Nanotechnology*, 2011, **22**, 245201.
18. L. B. Hu, H. S. Kim, J. Y. Lee, P. Peumans and Y. Cui, *ACS Nano*, 2010, **4**, 2955-2963.
19. D. S. Leem, A. Edwards, M. Faist, J. Nelson, D. D. C. Bradley and J. C. de Mello, *Adv Mater*, 2011, **23**, 4371-4375.
20. A. R. Madaria, A. Kumar, F. N. Ishikawa and C. W. Zhou, *Nano Res*, 2010, **3**, 564-573.
21. S. De, T. M. Higgins, P. E. Lyons, E. M. Doherty, P. N. Nirmalraj, W. J. Blau, J. J. Boland and J. N. Coleman, *ACS Nano*, 2009, **3**, 1767-1774.
22. V. Scardaci, R. Coull, P. E. Lyons, D. Rickard and J. N. Coleman, *Small*, 2011, **7**, 2621-2628.

23. R. M. Mutiso, Michelle C. Sherrott, Aaron R. Rathmell, Benjamin J. Wiley, and Karen I. Winey, *Acs Nano*, 2013, **7**, 7654-7663.
24. J. V. van de Groep, P. Spinelli and A. Polman, *Nano Lett*, 2012, **12**, 3138-3144.
25. I. N. Kholmanov, M. D. Stoller, J. Edgeworth, W. H. Lee, H. F. Li, J. H. Lee, C. Barnhart, J. R. Potts, R. Piner, D. Akinwande, J. E. Barrick and R. S. Ruoff, *Acs Nano*, 2012, **6**, 5157-5163.
26. S. W. Po-Chun Hsu, Hui Wu, Vijay K. Narasimhan, D. K. and H. R. L. Y. C., *Nat Commun*, 2013, **4**, 2522.
27. J. Lee, P. Lee, H. Lee, D. Lee, S. S. Lee and S. H. Ko, *Nanoscale*, 2012, **4**, 6408-6414.
28. D. Azulai, T. Belenkova, H. Gilon, Z. Barkay and G. Markovich, *Nano Lett*, 2009, **9**, 4246-4249.
29. A. R. Rathmell, S. M. Bergin, Y. L. Hua, Z. Y. Li and B. J. Wiley, *Adv Mater*, 2010, **22**, 3558-3563.
30. A. R. Rathmell, M. Nguyen, M. F. Chi and B. J. Wiley, *Nano Lett*, 2012, **12**, 3193-3199.
31. C. Sachse, L. Muller-Meskamp, L. Bormann, Y. H. Kim, F. Lehnert, A. Philipp, B. Beyer and K. Leo, *Org Electron*, 2013, **14**, 143-148.
32. H. B. Zhang, Q. Yan, W. G. Zheng, Z. X. He and Z. Z. Yu, *Acs Appl Mater Inter*, 2011, **3**, 918-924.
33. H. M. Kim, K. Kim, C. Y. Lee, J. Joo, S. J. Cho, H. S. Yoon, D. A. Pejakovic, J. W. Yoo and A. J. Epstein, *Appl Phys Lett*, 2004, **84**, 589-591.
34. L. Zhang, Lin Biao Wang, Kye Yak See, and J. Ma., *J Mater Sci*, 2013, **48**, 7757-7763.
35. J. Y. Zou, H. L. Yip, S. K. Hau and A. K. Y. Jen, *Appl Phys Lett*, 2010, **96**.
36. Y. Zhu, Z. Z. Sun, Z. Yan, Z. Jin and J. M. Tour, *Acs Nano*, 2011, **5**, 7686-7686.
37. M. G. Kang and L. J. Guo, *Adv Mater*, 2007, **19**, 1391-1396.
38. Z. Zhang, Zhang, X., Xin, Z., Deng, M., Wen, Y., & Song, Y., *Adv Mater*, 2013, **25**.
39. J.-S. Yu, Gwan Ho Jung, Jeongdai Jo, Jung Su Kim, Jun Woo Kim, Sun-Woo Kwak, Jong-Lam Lee, Inyoung Kim, and Dojin Kim., *Sol Energ Mat Sol C*, 2013, **109**, 142-147.
40. M. Layani, M. Grouchko, S. Shemesh and S. Magdassi, *J Mater Chem*, 2012, **22**, 14349-14352.
41. P. B. Catrysse and S. H. Fan, *Nano Lett*, 2010, **10**, 2944-2949.
42. I. Reinhold, C. E. Hendriks, R. Eckardt, J. M. Kranenburg, J. Perelaer, R. R. Baumann and U. S. Schubert, *J Mater Chem*, 2009, **19**, 3384-3388.
43. J. Perelaer, B. J. de Gans and U. S. Schubert, *Adv Mater*, 2006, **18**, 2101-2104.
44. H. S. Kim, S. R. Dhage, D. E. Shim and H. T. Hahn, *Appl Phys Mater*, 2009, **97**, 791-798.
45. M. L. Allen, M. Aronniemi, T. Mattila, A. Alastalo, K. Ojanpera, M. Suhonen and H. Seppa, *Nanotechnology*, 2008, **19**, 175201.
46. J. W. Chung, S. W. Ko, N. R. Bieri, C. P. Grigoropoulos and D. Poulidakos, *Appl Phys Lett*, 2004, **84**, 801-803.
47. S. Hong, J. Yeo, G. Kim, D. Kim, H. Lee, J. Kwon, H. Lee, P. Lee and S. H. Ko, *Acs Nano*, 2013, **7**, 5024-5031.
48. B. Kang, J. Yun, S. G. Kim and M. Yang, *Small*, 2013, **9**, 2111-2118.
49. M. Layani, M. Gruchko, O. Milo, I. Balberg, D. Azulay and S. Magdassi, *Acs Nano*, 2009, **3**, 3537-3542.
50. S. Magdassi, M. Grouchko, D. Toker, A. Kamyshny, I. Balberg and O. Millo, *Langmuir*, 2005, **21**, 10264-10267.
51. A. Kamyshny, M. Ben-Moshe, S. Aviezer and S. Magdassi, *Macromol Rapid Comm*, 2005, **26**, 281-288.
52. K. Higashitani, C. E. McNamee and M. Nakayama, *Langmuir*, 2011, **27**, 2080-2083.
53. M. Layani and S. Magdassi, *J Mater Chem*, 2011, **21**, 15378-15382.
54. Y. Galagan, J. E. J. M. Rubingh, R. Andriessen, C. C. Fan, P. W. M. Blom, S. C. Veenstra and J. M. Kroon, *Sol Energ Mat Sol C*, 2011, **95**, 1339-1343.
55. Y. Galagan, E. W. C. Coenen, S. Sabik, H. H. Gorter, M. Barink, S. C. Veenstra, J. M. Kroon, R. Andriessen and P. W. M. Blom, *Sol Energ Mat Sol C*, 2012, **104**, 32-38.
56. J. H. Zhang and B. Yang, *Adv Funct Mater*, 2010, **20**, 3411-3424.
57. N. Kwon, K. Kim, S. Sung, I. Yi and I. Chung, *Nanotechnology*, 2013, **24**, 235205.
58. K. Cheng, Z. G. Cui, Q. Q. Li, S. J. Wang and Z. L. Du, *Nanotechnology*, 2012, **23**.
59. R. D. Deegan, O. Bakajin, T. F. Dupont, G. Huber, S. R. Nagel and T. A. Witten, *Nature*, 1997, **389**, 827-829.
60. D. Soltman and V. Subramanian, *Langmuir*, 2008, **24**, 2224-2231.
61. A. M. J. van den Berg, A. W. M. de Laat, P. J. Smith, J. Perelaer and U. S. Schubert, *J Mater Chem*, 2007, **17**, 677-683.
62. J. Perelaer, P. J. Smith, C. E. Hendriks, A. M. J. van den Berg and U. S. Schubert, *Soft Matter*, 2008, **4**, 1072-1078.
63. J. B. Tan and Z. G. Lu, *Opt Express*, 2007, **15**, 790-796.
64. A. K. Geim and K. S. Novoselov, *Nat Mater*, 2007, **6**, 183-191.
65. K. S. Novoselov, A. K. Geim, S. V. Morozov, D. Jiang, Y. Zhang, S. V. Dubonos, I. V. Grigorieva and A. A. Firsov, *Science*, 2004, **306**, 666-669.
66. T. Fang, A. Konar, H. L. Xing and D. Jena, *Appl Phys Lett*, 2007, **91**.
67. J. B. Wu, M. Agrawal, H. A. Becerril, Z. N. Bao, Z. F. Liu, Y. S. Chen and P. Peumans, *Acs Nano*, 2010, **4**, 43-48.
68. M. Lotya, Y. Hernandez, P. J. King, R. J. Smith, V. Nicolosi, L. S. Karlsson, F. M. Blighe, S. De, Z. M. Wang, I. T. McGovern, G. S. Duesberg and J. N. Coleman, *J Am Chem Soc*, 2009, **131**, 3611-3620.
69. K. S. Kim, Y. Zhao, H. Jang, S. Y. Lee, J. M. Kim, K. S. Kim, J. H. Ahn, P. Kim, J. Y. Choi and B. H. Hong, *Nature*, 2009, **457**, 706-710.
70. X. S. Li, W. W. Cai, J. H. An, S. Kim, J. Nah, D. X. Yang, R. Piner, A. Velamakanni, I. Jung, E. Tutuc, S. K. Banerjee, L. Colombo and R. S. Ruoff, *Science*, 2009, **324**, 1312-1314.
71. M. Choucair, P. Thordarson and J. A. Stride, *Nat Nanotechnol*, 2009, **4**, 30-33.
72. K. V. Emtsev, A. Bostwick, K. Horn, J. Jobst, G. L. Kellogg, L. Ley, J. L. McChesney, T. Ohta, S. A. Reshanov, J. Rohrl, E. Rotenberg, A. K. Schmid, D. Waldmann, H. B. Weber and T. Seyller, *Nat Mater*, 2009, **8**, 203-207.
73. B. Y. Dai, L. Fu, L. Liao, N. Liu, K. Yan, Y. S. Chen and Z. F. Liu, *Nano Res*, 2011, **4**, 434-439.
74. G. Eda and M. Chhowalla, *Adv Mater*, 2010, **22**, 2392-2415.
75. Y. W. Zhu, W. W. Cai, R. D. Piner, A. Velamakanni and R. S. Ruoff, *Appl Phys Lett*, 2009, **95**, 103104.
76. N. R. Wilson, P. A. Pandey, R. Beanland, R. J. Young, I. A. Kinloch, L. Gong, Z. Liu, K. Suenaga, J. P. Rourke, S. J. York and J. Sloan, *Acs Nano*, 2009, **3**, 2547-2556.

77. W. W. Cai, Y. W. Zhu, X. S. Li, R. D. Piner and R. S. Ruoff, *Appl Phys Lett*, 2009, **95**, 123115.
78. V. C. Tung, M. J. Allen, Y. Yang and R. B. Kaner, *Nat Nanotechnol*, 2009, **4**, 25-29.
79. C. N. R. Rao, A. K. Sood *Graphene: Synthesis, Properties, and Phenomena*, Mar 4, 2013 edn., 2013.
80. J. T. Yuan, L. P. Ma, S. F. Pei, J. H. Du, Y. Su, W. C. Ren and H. M. Cheng, *Acs Nano*, 2013, **7**, 5647-5647.
81. I. Khrapach, F. Withers, T. H. Bointon, D. K. Polyushkin, W. L. Barnes, S. Russo and M. F. Craciun, *Adv Mater*, 2012, **24**, 2844-2849.
82. S. T. Hsiao, C. C. M. Ma, H. W. Tien, W. H. Liao, Y. S. Wang, S. M. Li and Y. C. Huang, *Carbon*, 2013, **60**, 57-66.
83. J. J. Liang, Y. Wang, Y. Huang, Y. F. Ma, Z. F. Liu, F. M. Cai, C. D. Zhang, H. J. Gao and Y. S. Chen, *Carbon*, 2009, **47**, 922-925.
84. B. Q. Yuan, L. M. Yu, L. M. Sheng, K. An and X. L. Zhao, *J Phys D Appl Phys*, 2012, **45**.
85. G. Cummins and M. P. Y. Desmulliez, *Circuit World*, 2012, **38**, 193-213.
86. A. Bachtold, M. Henny, C. Terrier, C. Strunk, C. Schonenberger, J. P. Salvetat, J. M. Bonard and L. Forro, *Appl Phys Lett*, 1998, **73**, 274-276.
87. Q. W. Li, Y. Li, X. F. Zhang, S. B. Chikkannanavar, Y. H. Zhao, A. M. Dangelewicz, L. X. Zheng, S. K. Doorn, Q. X. Jia, D. E. Peterson, P. N. Arendt and Y. T. Zhu, *Adv Mater*, 2007, **19**, 3358-3363.
88. M. M. J. Treacy, T. W. Ebbesen and J. M. Gibson, *Nature*, 1996, **381**, 678-680.
89. M. Terrones, *Annu Rev Mater Res*, 2003, **33**, 419-501.
90. A. Szabo, C. Perri, A. Csato, G. Giordano, D. Vuono and J. B. Nagy, *Materials*, 2010, **3**, 3092-3140.
91. J. Prasek, J. Drbohlavova, J. Chomoucka, J. Hubalek, O. Jasek, V. Adam and R. Kizek, *J Mater Chem*, 2011, **21**, 15872-15884.
92. N. N. Z. Y. C. Liu, J. D. Huang, B. M. Sun, Trans Tech Publications, Durnten-Zurich, Switzerland 2011.
93. R. Jasti and C. R. Bertozzi, *Chem Phys Lett*, 2010, **494**, 1-7.
94. Y. Gogotsi, J. A. Libera and M. Yoshimura, *J Mater Res*, 2000, **15**, 2591-2594.
95. B. Dan, G. C. Irvin and M. Pasquali, *Acs Nano*, 2009, **3**, 835-843.
96. S. L. Hellstrom, H. W. Lee and Z. N. Bao, *Acs Nano*, 2009, **3**, 1423-1430.
97. P. N. Nirmalraj, P. E. Lyons, S. De, J. N. Coleman and J. J. Boland, *Nano Lett*, 2009, **9**, 3890-3895.
98. N. Saran, K. Parikh, D. S. Suh, E. Munoz, H. Kolla and S. K. Manohar, *J Am Chem Soc*, 2004, **126**, 4462-4463.
99. T. V. Sreekumar, T. Liu, S. Kumar, L. M. Ericson, R. H. Hauge and R. E. Smalley, *Chem Mater*, 2003, **15**, 175-178.
100. D. S. Hecht, A. M. Heintz, R. Lee, L. B. Hu, B. Moore, C. Cucksey and S. Risser, *Nanotechnology*, 2011, **22**, 075201.
101. S. F. Pei, J. H. Du, Y. Zeng, C. Liu and H. M. Cheng, *Nanotechnology*, 2009, **20**.
102. Y. I. Lee, S. Kim, K. J. Lee, N. V. Myung and Y. H. Choa, *Thin Solid Films*, 2013, **536**, 160-165.
103. T. Wei, J. Ruan, Z. J. Fan, G. H. Luo and F. Wei, *Carbon*, 2007, **45**, 2712-2716.
104. A. J. Stapleton, R. A. Afre, A. V. Ellis, J. G. Shapter, G. G. Andersson, J. S. Quinton and D. A. Lewis, *Sci Technol Adv Mat*, 2013, **14**.
105. A. K. K. Kyaw, H. Tintang, T. Wu, L. Ke, C. Peh, Z. H. Huang, X. T. Zeng, H. V. Demir, Q. Zhang and X. W. Sun, *Appl Phys Lett*, 2011, **99**, 021107.
106. T. P. Tyler, R. E. Brock, H. J. Karmel, T. J. Marks and M. C. Hersam, *Adv Energy Mater*, 2011, **1**, 785-791.
107. D. S. Hecht, D. Thomas, L. B. Hu, C. Ladous, T. Lam, Y. Park, G. Irvin and P. Drzaic, *J Soc Inf Display*, 2009, **17**, 941-946.
108. S. Azoubel, S. Shemesh and S. Magdassi, *Nanotechnology*, 2012, **23**.